

# A multiscale approach to predict the effective conductivity of a suspension using the asymptotic homogenization method

Cite as: Phys. Fluids **34**, 062002 (2022); <https://doi.org/10.1063/5.0091451>

Submitted: 15 March 2022 • Accepted: 13 May 2022 • Accepted Manuscript Online: 15 May 2022 • Published Online: 02 June 2022

 Easwar M. K.,  A. Arockiarajan and  Anubhab Roy



View Online



Export Citation



CrossMark

## ARTICLES YOU MAY BE INTERESTED IN

[Insights into the dynamics of non-Newtonian droplet formation in a T-junction microchannel](#)  
Physics of Fluids **34**, 062001 (2022); <https://doi.org/10.1063/5.0092012>

[Heat transfer and fluid flow analysis in a realistic 16-generation lung](#)  
Physics of Fluids **34**, 061906 (2022); <https://doi.org/10.1063/5.0093912>

[Assessing effectiveness and comfortability of a two-layer cloth mask with a high-efficiency particulate air \(HEPA\) insert to mitigate COVID-19 transmission](#)  
Physics of Fluids **34**, 061703 (2022); <https://doi.org/10.1063/5.0094116>



## Physics of Fluids

Special Topic: Paint and Coating Physics

Submit Today!

# A multiscale approach to predict the effective conductivity of a suspension using the asymptotic homogenization method

Cite as: Phys. Fluids **34**, 062002 (2022); doi: 10.1063/5.0091451

Submitted: 15 March 2022 · Accepted: 13 May 2022 ·

Published Online: 2 June 2022






View Online



Export Citation



CrossMark

Easwar M. K.,<sup>1</sup>  A. Arockiarajan,<sup>1,2</sup>  and Anubhab Roy<sup>1,3,a)</sup> 

## AFFILIATIONS

<sup>1</sup>Department of Applied Mechanics, Indian Institute of Technology Madras, Chennai 600036, Tamil Nadu, India

<sup>2</sup>Ceramic Technologies Group-Center of Excellence in Materials and Manufacturing for Futuristic Mobility, Indian Institute of Technology Madras, Chennai 600036, Tamil Nadu, India

<sup>3</sup>Complex Systems and Dynamics Group, Indian Institute of Technology Madras, Chennai 600036, Tamil Nadu, India

<sup>a)</sup>Author to whom correspondence should be addressed: [anubhab@iitm.ac.in](mailto:anubhab@iitm.ac.in)

## ABSTRACT

This work aims to implement the asymptotic homogenization method (AHM) to predict the effective thermal/electrical conductivity for suspensions with aligned inclusions. Exploiting the substantial separation of length scales between the macroscopic and microscopic structures, multiscale modeling using the AHM capitalizes on the perturbations of the potential field caused due to the presence of an inclusion under a macroscopic loading used to predict the effective property. The analytical formulation for the thermal/electrical conductivity problem is derived, and subsequently, the finite element formulation required to solve the unit cell problem is described. The results obtained for a cylindrical inclusion are validated against known analytical solutions for both the dilute [Mori–Tanaka (MT)] and concentrated volume fractions ( $\phi$ ) of the inclusion. This study revealed that MT estimate and AHM agree well at  $\phi$  less than 0.4. However, in near-maximum packing fractions, the AHM results fared significantly better than MT when compared with known asymptotic forms [J. Keller, “Conductivity of a medium containing a dense array of perfectly conducting spheres or cylinders or nonconducting cylinders,” *J. Appl. Phys.* **34**, 991 (1963)]. The proposed AHM method is then implemented in structures with aligned spheroidal inclusions of various aspect ratios and conductivity ratios, thus providing a more generalized approach to predict the effective thermal/electrical conductivity. The results obtained are systematically benchmarked and validated against known analytical expressions.

Published under an exclusive license by AIP Publishing. <https://doi.org/10.1063/5.0091451>

## I. INTRODUCTION

In an era of heterogeneous materials, suspensions with anisotropic inclusions are used in various engineering applications ranging from polymer technology, paper pulp production, and pharmaceuticals to biomedical sectors. In addition to the above-mentioned applications, fibrous composites are integral to manufacturing components required for the automobile and aerospace industries. Though the concerned fields are plenty, a fundamental question needs to be addressed: does the material’s property suit the intended application? Computing and predicting the effective behavior of such materials have been a challenge in facilitating these applications.

As noted by Einstein,<sup>1</sup> suspensions with solid spherical particles enhance the viscosity of the base fluid. The effect of the dispersed phase on the transport coefficients of the suspension becomes more pronounced when their shape is now characterized by a large aspect

ratio.<sup>2–4</sup> The enhancement of the effective property due to the presence of these particles is not restricted to the viscosity of a fluid alone but also to other transport properties, such as diffusivity,<sup>5,6</sup> thermal conductivity,<sup>7,8</sup> and permeability.<sup>9</sup> Interaction among the different phases of the material occurs at a length scale much smaller than the characteristic length scale of the heterogeneous media. Multiscale models that exploit such differences in the length scale are used to compute the effective properties of the media using homogenization techniques, which include the widely used Mori–Tanaka (MT),<sup>10</sup> self-consistent,<sup>11</sup> and asymptotic homogenizations,<sup>12,13</sup> to name a few, that are widely used for elastic problems to find the effective property at dilute concentrations ( $\phi < 0.1$ ) of the inclusion.

The predominant focus of this work is on the problem of effective heat/current conducted through a quiescent suspension with aligned inclusions as a function of their aspect ratio and domain conductivity

ratios. Unlike the case of predicting the effective viscosity, the prediction of effective conductivity of the suspension is void of any particle kinematics; thus, the same methodology can be readily extended to find the effective conductivity for composite structures.

The earliest work on finding the effective conductivity was performed by Maxwell<sup>14</sup> where noninteracting spherical inclusions of volume fraction  $\phi$  and conductivity  $\kappa_{inc}$  were embedded in an infinite matrix space of conductivity  $\kappa_{mat}$ . The effective conductivity  $\kappa_{eff}$  is then given as a function of the conductivities and volume fractions. Extension to Maxwell's model was provided by Rocha and Acrivos<sup>15</sup> for spheroidal particles. These expressions were correct only to  $\mathcal{O}(\phi)$ , thus neglecting any particle–particle interactions. Jeffrey<sup>16</sup> extended Maxwell's model to  $\mathcal{O}(\phi^2)$  using probability density functions for dilute spherical inclusions.

Interestingly, it is possible to make analytical progress in the near-packing limit, where the nearest-neighbor lubrication interactions govern the interaction physics. In one of the earliest studies, Keller<sup>17</sup> considered interparticle interactions and gave analytical expressions for the conductivity of circular and spherical inclusions near the maximum packing fractions. Since the inclusions are perfect conductors, the effective conductivity is divergent for the limiting case where the solid spheres are in contact. A subsequent work by Batchelor and O'Brien<sup>18</sup> addressed the subtle double asymptotic limits—large but finite inclusion conductivity and the small gap between inclusions near the maximum packing fraction. They calculated the effective conductivity when the high-conductivity inclusions are in contact with each other via the dipole strength of the spherical particles suspended in a quiescent fluid. As an extension of Lord Rayleigh's work,<sup>19</sup> McPhedran and McKenzie<sup>20</sup> devised a method to calculate the conductivity of a system consisting of inclusion and matrix arranged in a simple cubic structure. Toward this, they developed a multipole expansion that predicted the conductivity with high accuracy even for close-packed spheres. At this close-packing limit, Sangani and Acrivos<sup>21</sup> modified Zuzovsky and Brenner's<sup>22</sup> methodology and subsequently solved a set of linear equations to compute the effective conductivity for spherical inclusions. The results obtained for the limiting case of maximum packing fraction were compared with Batchelor and O'Brien and differed only by a constant. Bonnecaze and Brady<sup>8</sup> developed a generalized method using an approach similar to the “Stokesian dynamics” for predicting effective conductivity. The technique involved the formulation of a capacitance matrix, which helped find the far-field and near-field effects with the necessary boundary conditions. Utilizing this obtained capacitance matrix, the effective conductivity was found by computing the particle dipoles.

Subsequently, the development of expressions to predict the effective conductivity for suspensions with anisotropic inclusions became a topic of interest. Formulation of the analytical expressions was deemed challenging due to the loss of symmetry in the shape of the inclusion. Chen and Acrivos<sup>23</sup> incorporated the results of Rocha and Acrivos<sup>15</sup> and Jeffrey<sup>16</sup> and developed expressions to predict the conductivity of a dilute system with highly conducting aligned spheroidal inclusions. Using the theory of slender body, Chen and Acrivos were able to predict the conductivity up to  $\mathcal{O}(\phi^2)$ . In another work, Lu and Kim<sup>24</sup> carried out a study to predict the effective conductivity of composites containing perfectly conducting aligned spheroidal inclusions. A virial expansion for  $\kappa_{eff}$  was obtained as a function of the inclusion volume fraction  $\phi$  up to  $\mathcal{O}(\phi^2)$ . A contemporary work by

Torquato and Lado<sup>25</sup> predicted the effective conductivity by using the perturbation expansion based on an  $n$ -point probability function. The results obtained were valid for dilute dispersion of ellipsoids.

Further investigations were carried out to predict the effective property of microstructures with spheroidal inclusions over the entire spectrum of inclusion volume fractions. Lu and Lin<sup>26</sup> extended Lu and Kim's methodology to the more general case of finite inclusion conductivity and thus provided analytical expressions to compute the effective conductivity for aligned spheroidal inclusions considering the interactions between a pair of inclusions. A two-particle boundary-value problem was solved by using the boundary collocation method to capture the near-field interactions and hence the thermal dipole moments. The pair distribution function, which depends on the microstructure of the system under consideration, is computed by adopting a well-stirred model. The results obtained by the numerical simulation and the pair distribution function were then subsequently used to derive the expressions for  $\kappa_{eff}$ . Even though there are a considerable amount of contributions by various authors over the years, the absence of a more generalized method or lack thereof, which predicts the effective conductivity, irrespective of the shape and size of the inclusion, motivates us to explore the feasibility of asymptotic homogenization to predict the effective conductivity.

The asymptotic homogenization method (AHM)<sup>12,27,28</sup> exploits the sharp separation between the microscale and macroscale to decouple spatial variations and employs asymptotic expansions of the fields. This approach, under the assumption of periodicity in the microstructure, yields a set of effective governing equations, which describe the macroscale mechanics of the heterogeneous material. A detailed review of the AHM can be found in these articles.<sup>29,30</sup> Many authors have employed the AHM to predict the effective property for multifunctional layered composite materials<sup>31–33</sup> and were validated against existing analytical expressions for the same. The AHM is also used to predict effective transport properties such as the effective fluid permeability<sup>34–36</sup> and diffusion coefficient<sup>37,38</sup> for systems with periodic structures. Rubinstein and Torquato<sup>34</sup> computed the effective fluid permeability through a porous media using the AHM, while Auriault and Lewandowska<sup>38</sup> used the AHM to predict the effective diffusion coefficient for a periodic porous media. A more recent work<sup>39</sup> compared the accuracy of the results predicted by the AHM and the representative volume element method in thermal composites, thus proving the efficacy and robustness of the AHM. Though the derivations required to find the effective property expression are mathematically extensive, the use of the finite element (FE) method helps simplify the solving procedure. Such solving schemes have been adopted,<sup>40–42</sup> and the accuracy of the results obtained has been verified. A brief overview of the literature survey is shown in Table I.

As shown in Mori–Tanaka, Maxwell's, and subsequent studies, the models predict the effective property very well for dilute packing limits while failing to capture the interparticle interactions at semidilute and maximum packing fractions. Though the work by Lu and Lin<sup>26</sup> predicted the effective property very well for aligned spheroidal inclusions over the entire spectrum of packing fractions, the available expressions are an implicit function of both the conductivity ratio and the aspect ratio of the inclusion. Thus, deriving a closed-form solution for an entirely new combination of aspect ratio and conductivity involves a lot of mathematical rigor. Taking into account the abovesaid limitations, and with an aim to provide a more generalized method to

TABLE I. Overview of literature survey.

Domain	Literature	Remarks
Mean-field methods	Maxwell, <sup>14</sup> self-consistent, <sup>11</sup> Mori–Tanaka <sup>10</sup>	Single inclusion in infinite matrix space
Analytical estimates	Keller, <sup>17</sup> Jeffrey, <sup>16</sup> Batchelor and O’Brien, <sup>18</sup> McPhedran and McKenzie, <sup>20</sup> Sangani and Acrivos, <sup>21</sup> and Bonnecaze and Brady <sup>8</sup>	Spherical inclusions
	Rocha and Acrivos, <sup>15</sup> Chen and Acrivos, <sup>23</sup> Lu and Kim, <sup>24</sup> Torquato and Lado, <sup>25</sup> and Lu and Lin <sup>26</sup>	Spheroidal inclusions
Asymptotic homogenization	Rubinstein and Torquato, <sup>34,37</sup> Auriault and Lewandowska, <sup>38</sup> Takano <i>et al.</i> , <sup>35</sup> Song and Youn, <sup>36</sup> Andreassen and Andreassen, <sup>40</sup> Fantoni <i>et al.</i> , <sup>41</sup> Dutra <i>et al.</i> , <sup>42</sup> and Lee and Lee <sup>39</sup>	Application of the AHM in predicting effective transport coefficients

predict the effective conductivity for the complete range of packing fractions and to capture the interparticle interactions, which occur close to maximum packing fractions, we propose this method, which uses the robustness of the AHM with the efficacy of the FE solutions to predict the effective conductivity.

In Sec. II A, the multiscale formulation for the effective conductivity problem is derived, while in Sec. II B, the FE formulation required to solve for the same is described. In Sec. III A, the results obtained are benchmarked against the known analytical results for a cylindrical inclusion and then the study is further extended to inclusions of more general shapes in Sec. III B.

## II. MULTISCALE MODELING

In this work, we consider composites with a regular structure, thus making it possible to use periodic homogenization. To this end, a periodic microstructure is assumed for the composite, made up of many repetitive unit cells. The length scale associated with the repetitive unit cell is well separated from that of the macrostructure. The unit cell entails the geometric and material properties at the microscopic level, thus significantly influencing the macroscopic behavior of the composite.

As shown in Fig. 1, we consider the unit cell to be made up of an inclusion within a continuous media (matrix/suspension phase). The

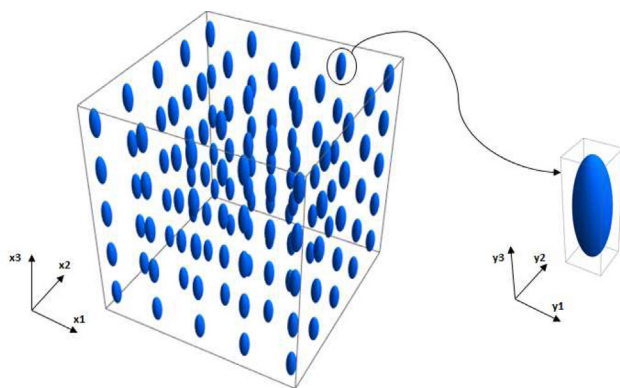


FIG. 1. Continuous media and the corresponding unit cell.

interface between an inclusion and a continuous phase is assumed to be perfect (neglecting any interface effects). Since the unit cells are seen as the building blocks of the composite, any geometric or material property associated with the unit cell will repeat over a constant length  $Y$ , which is termed as its periodicity. For a heterogeneous material domain  $\Omega$ , the periodicity of the material can be mathematically represented by

$$\phi(\mathbf{x} + \mathbf{Y}) = \phi(\mathbf{x}) \quad \forall \mathbf{x} \quad \text{and} \quad \forall (\mathbf{x} + \mathbf{Y}) \in \Omega. \quad (1)$$

Based on these assumptions and the existence of a distinguishable length scale, the effective properties of the heterogeneous media can be determined by solving a large but finite number of unit cell problems.

### A. Asymptotic homogenization

If we assign a coordinate system  $\mathbf{x}$  defining the macroscopic length scale and a coordinate system  $\mathbf{y}$  to define the microscopic length scale, then the two sets of coordinates are related through the scale separation parameter  $\varepsilon$  ( $\varepsilon \ll 1$ ) by

$$y_i = \frac{x_i}{\varepsilon}. \quad (2)$$

The  $\mathbf{x}$  is the slow or global variable, which describes the long-range interactions, while  $\mathbf{y}$  is the fast or local variable that describes the short-range interactions. It is, in a sense, to be understood that the variations that macroscopically occur are being captured by the  $\mathcal{O}(1)$  term, that is, the macroscopic variable  $x$ , but the variations that occur at the microscopic length scale are of the  $\mathcal{O}(\varepsilon)$  and can only be captured by a finer length scale  $y$ , which scales the macroscopic length scale as  $1/\varepsilon$ , represented by Eq. (2).

We now consider the problem of thermal/electrical conductivity in a heterogeneous body with domain  $\Omega$ , defined by the following equations:

1. Constitutive equation

$$J_i^c(\mathbf{x}) = \kappa_{ij}^c(\mathbf{x}) E_j^c(\mathbf{x}) \quad \text{in} \quad \Omega, \quad (3)$$

2. Balance law

$$J_{i,i}^c(\mathbf{x}) = 0 \quad \text{in} \quad \Omega, \quad (4)$$

3. Definition of potential gradient

$$E_i^\varepsilon(\mathbf{x}) = -V_{,i}^\varepsilon(\mathbf{x}) \quad \text{in } \Omega, \tag{5}$$

4. Boundary condition and jumps

$$\llbracket J_i^\varepsilon n_i \rrbracket = 0 \quad \text{on the interface}, \tag{6}$$

$$\llbracket V^\varepsilon \rrbracket = 0 \quad \text{on the interface}, \tag{7}$$

where  $J_i(\mathbf{x})$ ,  $E_i(\mathbf{x})$ , and  $\kappa_{ij}(\mathbf{x})$  denote the Cartesian components of heat flux/electric current density, the temperature gradient/electric field, and the conductivity (thermal/electrical) tensor, and  $V$  is the temperature/electric potential, while superscript  $\varepsilon$  denotes that the macroscopic quantities have a dependency on microstructure.  $(\cdot)_{,i}$  denotes the spatial gradient of the field of interest along with the  $i$ th direction. Using relations (5) and (3) in relation (4), we get

$$-(\kappa_{ij}^\varepsilon(\mathbf{x})V_{,j})_{,i} = 0. \tag{8}$$

Owing to the  $Y$ -periodicity of the material, the conductivity tensor  $\kappa$  obeys the following property:

$$\kappa_{ij}^\varepsilon(\mathbf{x} + \mathbf{Y}) = \kappa_{ij}^\varepsilon(\mathbf{x}), \quad \forall \mathbf{x} \in \Omega. \tag{9}$$

Thus, the variation of the conductivity tensor depends only on the microscopic variable  $\mathbf{y}$ , and hence, it is evident that the solution to the problem depends on both the macrolength and the microlength scales. Furthermore, assuming an analogous periodical perturbation on quantities describing the thermal/electrical behavior of the body imposed upon by the periodicity of the material characteristics, a two-scale asymptotic expansion of the solution  $V(\mathbf{x})$  is considered in terms of the macrovariables and microvariables

$$V^\varepsilon(\mathbf{x}) = V_0(\mathbf{x}, \mathbf{y}) + \varepsilon V_1(\mathbf{x}, \mathbf{y}) + \varepsilon^2 V_2(\mathbf{x}, \mathbf{y}) \dots, \tag{10}$$

where  $V_i$  stands for the periodically varying temperature/electrical potential perturbations due to the microstructure. Likewise, a similar expansion for electric field and current density vectors can be written as

$$\mathbf{E}^\varepsilon(\mathbf{x}, \mathbf{y}) = \mathbf{E}_0(\mathbf{x}, \mathbf{y}) + \varepsilon \mathbf{E}_1(\mathbf{x}, \mathbf{y}) + \varepsilon^2 \mathbf{E}_2(\mathbf{x}, \mathbf{y}) + \varepsilon^3 \mathbf{E}_3(\mathbf{x}, \mathbf{y}) \dots, \tag{11}$$

$$\mathbf{J}^\varepsilon(\mathbf{x}, \mathbf{y}) = \mathbf{J}_0(\mathbf{x}, \mathbf{y}) + \varepsilon \mathbf{J}_1(\mathbf{x}, \mathbf{y}) + \varepsilon^2 \mathbf{J}_2(\mathbf{x}, \mathbf{y}) + \varepsilon^3 \mathbf{J}_3(\mathbf{x}, \mathbf{y}) \dots \tag{12}$$

Given Eq. (10), in order to determine electric field asymptotes in Eq. (11), the chain rule is exploited as follows:

$$V_{,i} = V_{,i(x)} + \frac{1}{\varepsilon} V_{,i(y)}, \tag{13}$$

where  $V_{,i(x)} \equiv \frac{\partial V}{\partial x_i}$  and  $V_{,j(y)} \equiv \frac{\partial V}{\partial y_j}$ . Making use of Eqs. (10) and (13), Eq. (8) is rewritten as

$$\begin{aligned} & -(\kappa_{ij}(\mathbf{y})V_{o_{j(x)}})_{,i(x)} - \frac{1}{\varepsilon}(\kappa_{ij}(\mathbf{y})V_{o_{j(x)}})_{,i(y)} - \frac{1}{\varepsilon}(\kappa_{ij}(\mathbf{y})V_{o_{j(y)}})_{,i(x)} \\ & - \frac{1}{\varepsilon^2}(\kappa_{ij}(\mathbf{y})V_{o_{j(y)}})_{,i(y)} - \varepsilon(\kappa_{ij}(\mathbf{y})V_{1_{j(x)}})_{,i(x)} - (\kappa_{ij}(\mathbf{y})V_{1_{j(x)}})_{,i(y)} \\ & - (\kappa_{ij}(\mathbf{y})V_{1_{j(y)}})_{,i(x)} - \frac{1}{\varepsilon}(\kappa_{ij}(\mathbf{y})V_{1_{j(y)}})_{,i(y)} = 0. \end{aligned} \tag{14}$$

Grouping the results in  $\mathcal{O}(\varepsilon)$ , the leading order terms are given by

$$-(\kappa_{ij}(\mathbf{y})V_{o_{j(y)}}) = 0. \tag{15}$$

For the existence of a solution, Eqs. (15) and (16) must satisfy the solvability condition.<sup>12</sup> Equation (15) identically satisfies the solvability condition, and thus,  $V_0$  is only a function of the macroscopic variable  $\mathbf{x}$ . Grouping the next order terms in  $\varepsilon$ , we get

$$-(\kappa_{ij}(\mathbf{y})V_{o_{j(x)}})_{,i(y)} - (\kappa_{ij}(\mathbf{y})V_{1_{j(y)}})_{,i(y)} = 0. \tag{16}$$

For Eq. (16) to satisfy the solvability condition, the solution  $V_1$  takes the form

$$V_1(\mathbf{x}, \mathbf{y}) = \chi_j(\mathbf{y})V_{o_{j(x)}}, \tag{17}$$

where  $\chi$  is the homogenization function and is periodic with a periodicity of  $Y$ . Utilizing the results obtained in Eqs. (16) and (17) in Eq. (8), we get the governing equation or the cell problem, which needs to be solved to find  $\chi$ ,

$$-(\kappa_{ij}(\mathbf{y}) + \kappa_{ik}(\mathbf{y})\chi_{j,k(y)}(\mathbf{y}))_{,i(y)} = 0. \tag{18}$$

The volumetric average of a quantity  $a(\mathbf{x}, \mathbf{y})$  over  $Y$  is defined by

$$a^H = \frac{1}{|Y|} \int_Y a(\mathbf{x}, \mathbf{y}) dY. \tag{19}$$

Using the results from Eqs. (3), (11), and (18), one can get the effective conductivity  $\kappa^H$  as

$$\kappa_{ij}^H = \frac{1}{|Y|} \int_Y (\kappa_{ij}(\mathbf{y}) + \kappa_{ik}(\mathbf{y})\chi_{j,k(y)}(\mathbf{y})) dY. \tag{20}$$

**B. Numerical implementation**

The cell problem as defined by Eq. (18) can be numerically solved using FE. To predict the effective conductivity matrix, we consecutively apply a unit potential in each direction; thus, we have three unique solutions to the homogenization function. The homogenization function  $\chi$  within a given element, thus, can be written in matrix form as

$$[\chi(\mathbf{y})] = [\chi^{f^1} \quad \chi^{f^2} \quad \chi^{f^3}]_{1 \times 3}, \tag{21}$$

where  $\chi^{f^i}$  is the solution of the cell problem for the applied unit potential difference along the direction  $y_i$ . The degree of freedom vector  $d_i$  containing the nodal potentials corresponding to the applied unit potential difference along with  $y_i$  is obtained by the usual Lagrange interpolation functions. This gives the representation of  $\chi$  as

$$[\chi(\mathbf{y})]_{1 \times 3} = [\mathbf{N}(\mathbf{y})]_{1 \times n} \{d\}_{n \times 3}, \tag{22}$$

where  $[\mathbf{N}]$  is the matrix of the standard Lagrange shape functions, and  $n$  is the number of degrees of freedom per element. The variational form of the governing Eq. (18) is given as

$$\int_Y (\kappa_{ij}(\mathbf{y}) + \kappa_{ik}(\mathbf{y})\chi_{j,k}(\mathbf{y}))\nu_j dY = 0, \tag{23}$$

where  $\nu$  is the variation in  $\chi$ . Using the matrix notations, the variational form can be rewritten as

$$\int_Y \left( [B]^T [D] + [B]^T [D] [B] \{d\} \right) dY = 0. \tag{24}$$

The nodal solution of the homogenization function  $\chi$  is obtained by solving Eq. (24). The system of linear equations, which is to be solved, reduces to



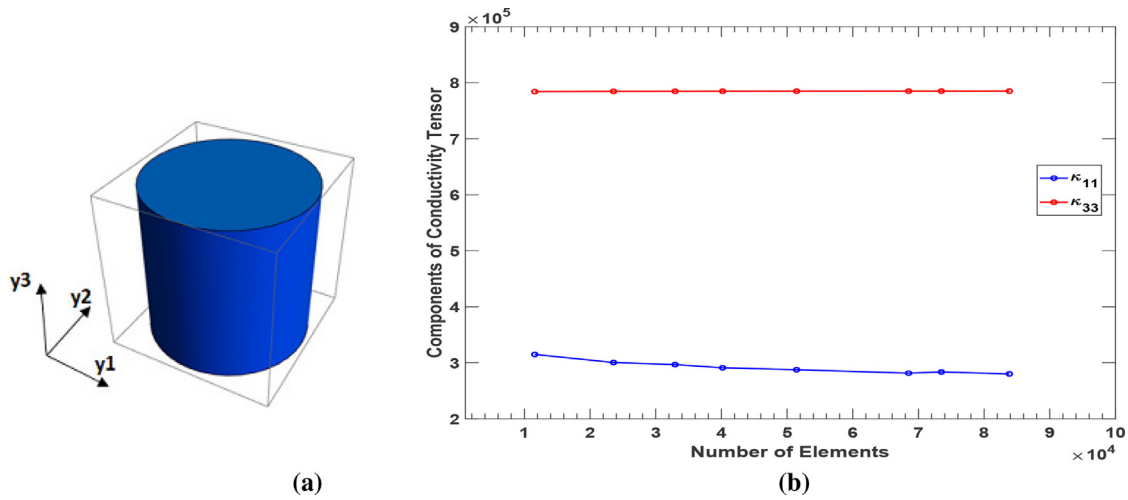


FIG. 2. (a) Unit cell with a cylindrical inclusion. (b) Mesh convergence study for a unit cell with cylindrical inclusion for  $\phi = \pi/4$  and  $\kappa_r = 10^6$ .

$$[K]\{d\} - \{F\} = \{0\}, \tag{25}$$

where

$$\{F\} = - \int_Y [B]^T [D] dY, \quad [K] = \int_Y [B]^T [D] [B] dY, \tag{26}$$

$$[B]_{3 \times n} = [L]_{3 \times 1} [N]_{1 \times n}.$$

$[D]_{3 \times 3}$  contains the material conductivities, and  $[L]$  denotes the matrix of differential operators. Having computed  $[N]$  and by consequence  $V_1$  from Eq. (17), one can derive the effective material coefficients, according to

$$\kappa_{ij}^H = \frac{1}{|Y|} \int_Y [D] ([I] + [B]\{d\}) dY. \tag{27}$$

In-house codes were written in MATLAB® to compute the effective conductivity given by Eq. (27). The developed code is initially benchmarked for a cylindrical inclusion and then further extended to spheroidal inclusions of varying aspect ratios and conductivity ratios.

### III. RESULTS AND DISCUSSION

#### A. Cylindrical inclusion

In order to validate the proposed model, as an initial study, suspensions with cylindrical inclusions in a simple cubic arrangement are considered. The simulations can be readily extended to other prevalent arrangements (BCC and FCC) of the inclusions as well.  $y_3$  is considered to be the axis of symmetry as shown in Fig. 2(a). For the simulations, conductivities of both the inclusion ( $\kappa_{inc}$ ) and continuous phase ( $\kappa_{mat}$ ) are considered isotropic and  $\kappa_{inc} \gg \kappa_{mat}$ . The mesh convergence study was carried out until the component-wise difference between the computed effective property for the current mesh and the consecutive finer mesh is less than a specified tolerance value ( $10^{-2}$ ) as given in literature.<sup>43</sup> From Fig. 2(b), for this set of simulations, 85 000 eight-noded brick elements were deemed sufficient. The simulations were run for three conductivity ratios  $\kappa_r = (\kappa_{inc}/\kappa_{mat})$ , as mentioned in Table II. Due to very high orders of difference in the magnitudes of

the conductivities of the constituent phases, the results are represented in a log-log plot for the sake of clarity.

Figures 3(a) and 3(b) compare the results between existing analytical estimates and the present model. In this plot and all subsequent plots, the values obtained for conductivity ratios  $10^2$ ,  $10^4$ , and  $10^6$  are represented by blue, red, and black colors, respectively. In Fig. 3(a), the ratio of the component of conductivity along the cylindrical axis ( $\kappa_{33}^H$ ) to  $\kappa_{mat}$  is plotted as a function of the inclusion volume fraction. As seen from the plot, the results predicted by the present model and the Mori-Tanaka estimate agree very well over the entire range of volume fractions. In Fig. 3(b), the results obtained from simulations in the plane of symmetry,  $\kappa_{11}^H (= \kappa_{22}^H)$ , agree well with the Mori-Tanaka estimate for dilute concentrations of the inclusion ( $\phi < 0.1$ ).

As the concentration of the inclusion increases and approaches the dense packing limit ( $\phi > 0.5$ ), the deviation of the results is observed, which can be explained to be a consequence of the particle-particle interactions, which play a significant role in the effective property of the material. Being a mean-field method, the Mori-Tanaka estimate fails to capture these interactions and hence underpredicts the effective conductivity. The presence of an inclusion will cause a disturbance to the applied potential. The flux field can now be seen as a superposition of the applied field and the perturbed field caused due to the presence of the inclusion. The strength of the perturbed field proportionally varies with the conductivity ratio of the inclusion and matrix. When the particles are close enough, the perturbations caused to the field become prominent and subsequently enhance the effective conductivity. The AHM, which computes the effective property using

TABLE II. Conductivity ratio of systems considered and relevant systems in use.

Conductivity ratio	Relevant systems
$10^2$	Copper particles in ethanol
$10^4$	Graphite particles in aqueous KOH solutions <sup>44</sup>
$10^6$	Carbon nanotubes in epoxy matrix <sup>45</sup>

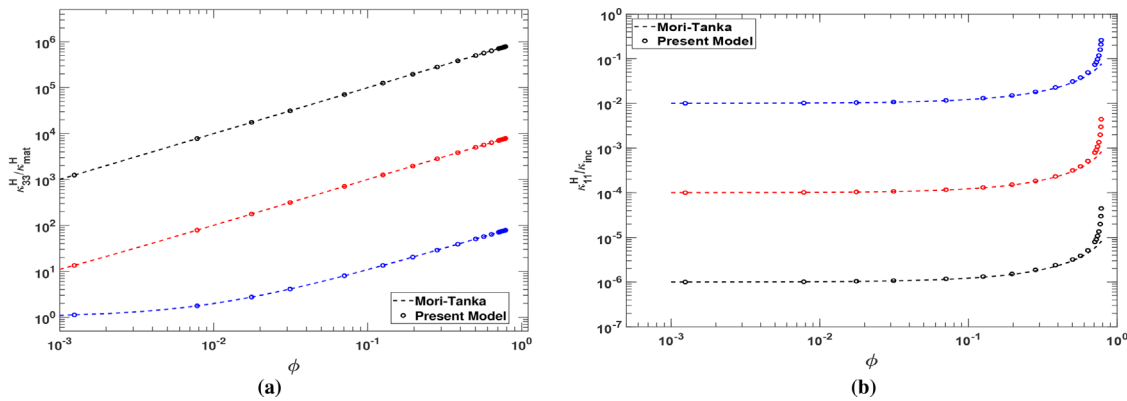


**FIG. 3.** Ratio of (a)  $\kappa_{33}^H$  to  $\kappa_{mat}$  and (b)  $\kappa_{11}^H$  to  $\kappa_{mc}$  as a function of volume fraction  $\phi$  of cylindrical inclusions in a simple cubic arrangement. The dashed lines represent the Mori–Tanaka estimate, and dash–dot represents Keller’s (1963)<sup>17</sup> expression, while the results from present model are plotted using the circle symbol for the different conductivity ratios. The values obtained for conductivity ratios  $10^2$ ,  $10^4$ , and  $10^6$  are represented by blue, red, and black colors, respectively.

the field perturbations caused due to the presence of an inclusion (18), can more accurately capture the variations in the field and, hence as a consequence, predict the enhancement of effective conductivity.

The ratio of  $\kappa_{11}^H$  to  $\kappa_{mat}$  is plotted as a function of the deviation of the inclusion packing fraction from the maximum packing fraction is shown in Fig. 4. By using Keller’s expression, which is valid for volume fractions close to the maximum packing limit and infinitely conducting inclusions, the influence of the particle–particle interactions on the effective conductivity is ascertained. As noted by Keller, close to the maximum packing fraction,  $\kappa_{eff}$  solely depends on the interparticle distance

$$\kappa_{eff}/\kappa_{mat} = \pi^3/2(\pi/4 - \phi)^{1/2} + \dots, \quad \pi/4 - \phi \ll 1. \quad (28)$$

From the figure, it can be seen that the AHM results obtained for various conductivity ratios approach Keller’s result for a conductivity ratio of  $10^4$  [Eq. (28)]. Hence, the agreement of the present model with the existing analytical estimates establishes the feasibility of the proposed approach.

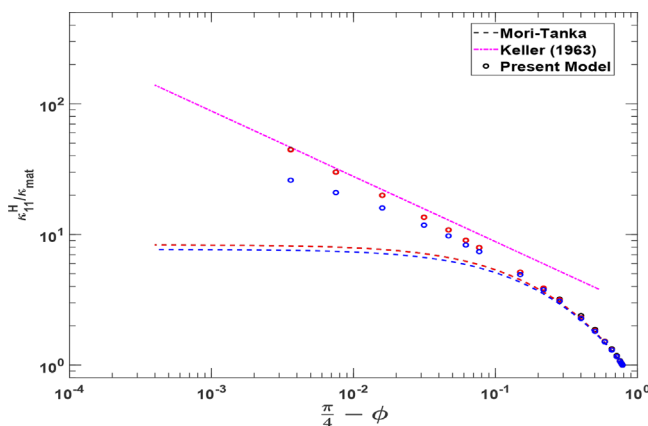


**FIG. 4.** Ratio of  $\kappa_{11}^H$  to  $\kappa_{mat}$  as a function of deviation from the maximum packing fraction  $\pi/4$  (simple cubic arrangement of cylindrical inclusions). The dashed–dot line represents Keller’s (1963)<sup>17</sup> results, while the results from present model are plotted using the circle symbol for the different conductivity ratios. The color scheme is the same as mentioned in Fig. 3.

### B. Spheroidal inclusion

In this section, heterogeneous media with aligned spheroidal inclusions, mathematically described using the general ellipsoidal equation given by

$$\frac{y_1^2}{a^2} + \frac{y_2^2}{b^2} + \frac{y_3^2}{c^2} + 1 = 1, \quad (29)$$

are considered.  $a$ ,  $b$ , and  $c$  are the three semiaxes of a general ellipsoid. Setting  $a = b > c$  reduces the ellipsoid to an oblate spheroid, while setting  $a = b < c$  reduces it to a prolate spheroid. As shown in Figs. 5(a)–5(c),  $y_3$  is taken as the axis of symmetry.

The simulations are carried out for the special case of spherical inclusion for all the conductivity ratios specified in Table II, where  $a = b = c$  as shown in Fig. 5(c). Four-noded tetrahedral elements were used for meshing, and, as seen from the convergence plot in Fig. 6,  $10^5$  elements were deemed sufficient for a system having a conductivity ratio of  $10^6$ .

The plot of the ratio of  $\kappa_{11}^H$  to  $\kappa_{mat}$  as a function of  $\phi$  is shown in Fig. 7 for a conductivity ratio of  $10^2$ . The obtained results are compared with the values predicted by Bonneau and Brady<sup>8</sup> using an approach similar to Stokesian dynamics, and it is clearly evident that the results agree very well. In our previous discussion on cylindrical inclusions, we observed that AHM could accurately capture the asymptotic behavior of effective conductivity in the maximum packing limit. We further investigate this ability of the AHM for spherical

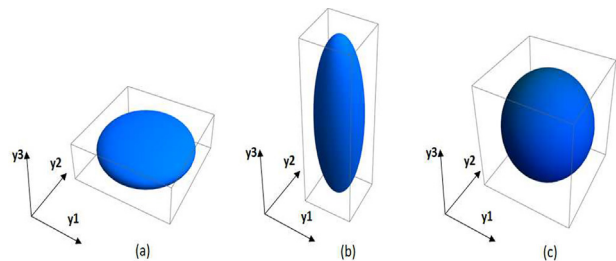


**FIG. 5.** Unit cell with (a) oblate, (b) prolate, and (c) spherical inclusions.

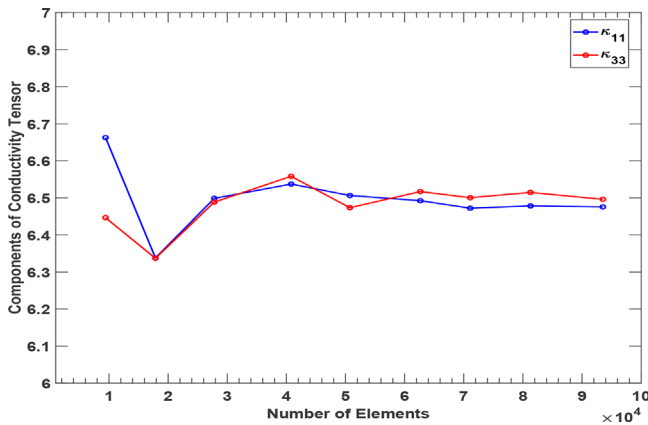


FIG. 6. Mesh convergence study for a unit cell with a spherical inclusion for  $\phi = 0.5$  and  $\kappa_r = 10^6$ .

inclusions. A plot of the ratio of  $\kappa_{11}^H$  to  $\kappa_{inc}$  as a function log of the inverse of the deviation of  $\phi$  from the maximum packing fraction  $\pi/6$  is shown in Fig. 8(a) for the conductivity ratios mentioned in Table II. It is interesting to note that the results predicted by the AHM agree well with the Torquato and Lado<sup>25</sup> up to dilute packing fractions ( $\phi < 0.1$ ). At semidilute and concentrated packing regimes ( $\phi > 0.3$ ), the AHM predictions deviate from the Torquato and Lado curves due to the interparticle effect, which is not taken into consideration by the former.

The scenario of  $\phi$  asymptotically approaching the maximum packing limit, as noted by various authors, is intriguing, especially for systems with highly conducting inclusions. This condition involves the limit of the gap between any two inclusions asymptotically reaching 0 while the conductivity ratio,  $\kappa_r$ , is  $\gg 1$ . The plot in Fig. 8(b), which shows the ratio  $\kappa_{11}^H$  to  $\kappa_{mat}$  as a function of the deviation of  $\phi$  from maximum packing fraction  $\pi/6$ , is used to compare the results predicted by the present model for this intriguing case

$$\kappa_{eff} / \kappa_{mat} = -\pi/2 \times \log(\pi/6 - \phi) + \dots, \quad \pi/6 - \phi \ll 1. \quad (30)$$

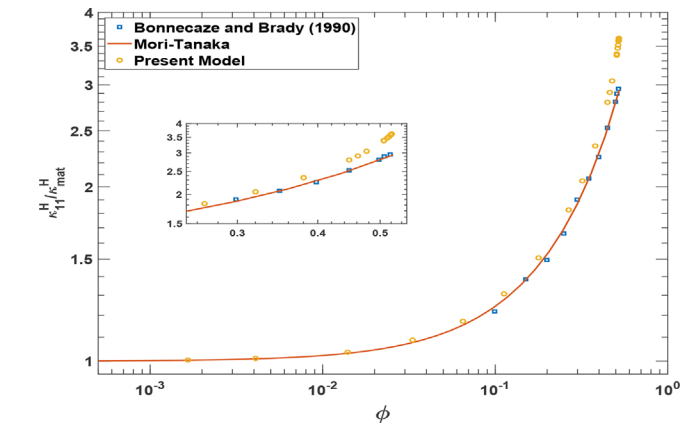
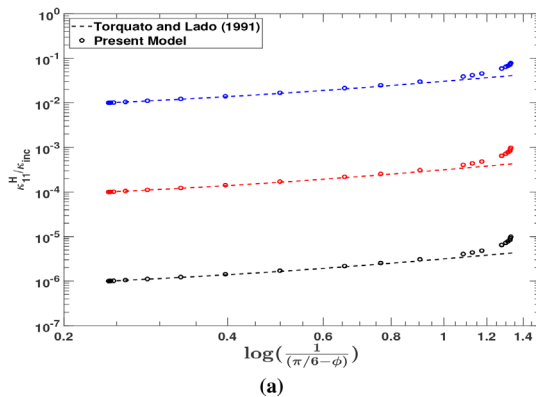


FIG. 7. Ratio of  $\kappa_{11}^H$  to  $\kappa_{mat}$ , for a simple cubic arrangement of spherical inclusions, as a function of  $\phi$  for a conductivity ratio of  $10^2$  comparing the present model to the results of Bonnecaze and Brady (1990)<sup>8</sup> and that of predictions from the Mori-Tanaka theory. The inset shows ratio of  $\kappa_{11}^H$  to  $\kappa_{mat}$  for  $\phi > 0.25$ .

Batchelor and O'Brien<sup>18</sup> extended Keller's<sup>17</sup> [Eq. (30)] analysis to spherical inclusions of large but finite conductivity. They pointed out that due to the dual asymptotic limits, the largeness of the conductivity ratio, and the smallness of the interstitial gap, it is not an obvious conclusion whether the effective conductivity would approach  $\kappa_{mat}$  or  $\kappa_{inc}$ . Realizing that near-maximum packing fraction interactions are lubrication-dominated, they obtained an integral equation that needed to be solved to evaluate the heat flux. They managed to get an expression for the effective conductivity in the limit of touching spheres that varied as the logarithm of the conductivity ratio. The expression given by Batchelor and O'Brien<sup>18</sup> and the subsequent expression given by Sangani and Acrivos<sup>21</sup> differ by an  $\mathcal{O}(1)$  constant

$$\kappa_{eff} / \kappa_{mat} \sim \pi \times \log(\kappa_r) - 5.91. \quad (31)$$

The above expression is used as an asymptotic check for the effective conductivity obtained from the AHM in the scenario of dense suspension. In order to capture the dual asymptotic limits, for a given

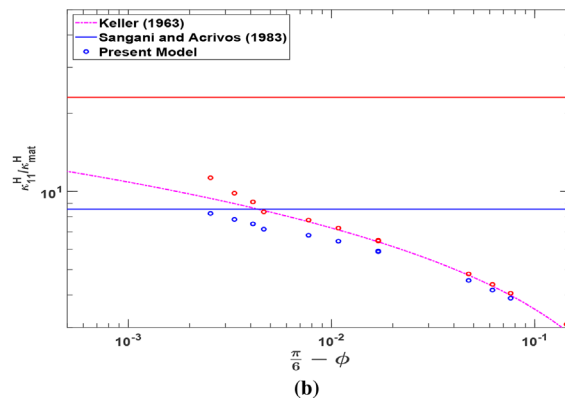


FIG. 8. Ratio of (a)  $\kappa_{11}^H$  to  $\kappa_{inc}$  and (b)  $\kappa_{11}^H$  to  $\kappa_{mat}$  as a function of deviation from maximum packing fraction  $\pi/6$ . The solid lines represent the effective conductivity predicted by Sangani and Acrivos (1983) at maximum packing limit, and dash-dot represents Keller's (1963)<sup>17</sup> expression, while the results from present model are plotted using the circle symbol for the different conductivity ratios. The color scheme is same as mentioned in Fig. 3.



TABLE III. Considered spheroidal shapes and their respective aspect ratios.

S. No	Spheroidal shape	Aspect ratio
1	Oblate	0.1
2		0.2
3		0.5
4	Prolate	2.0
5		5.0
6		10.0

conductivity ratio, the gap between the two spheres is reduced. For the maximum volume fraction under consideration, the gap between the neighboring spheres is of  $\mathcal{O}(10^{-3})$ . From the plot, we could see that for a conductivity ratio of  $10^2$  and almost touching spheres, the results predicted by the AHM approach the asymptotic estimate provided by Sangani and Acrivos. On the other hand, for a conductivity ratio of  $10^4$ , there is a slight deviation of the predicted result from Keller's curve toward the Sangani and Acrivos estimate. The significant difference between the two results, AHM and Sangani and Acrivos, could

be due to the limitations of the numerical model to obtain an even smaller separation between the two neighboring inclusions.

It is interesting to note that, though the analytical formulation can be easily extended to higher powers in  $\epsilon$ , from the aforementioned discussions for the spherical and cylindrical inclusions, it is clearly seen that the algebra, which is based on the first-order theory in  $\epsilon$ , deems sufficient to predict the effective properties, thus justifying the truncation of the formulation.

The work is now extended to anisotropic inclusions, exploring spheroidal particles of aspect ratios as mentioned in Table III. A parametric study is carried out for all the combinations of the aspect ratios mentioned in Table III and conductivity ratios specified in Table II. For this study, four-noded tetrahedral elements were used for meshing. The convergence plot for the inclusion aspect ratios of 0.1 and 10 and a conductivity ratio of  $10^6$  is shown in Figs. 9(a) and 9(b). It is concluded that  $9 \times 10^4$  and  $1.3 \times 10^5$  elements are required for running the respective simulations.

For all the subsequent computations, we consider  $\phi < 0.1$  as a dilute packing regime while  $\phi > 0.3$  is considered as the dense packing regimes. Figures 10–12 show plots of the effective conductivity along with the characteristic dimension of the spheroid (along the  $y_1$  axis for

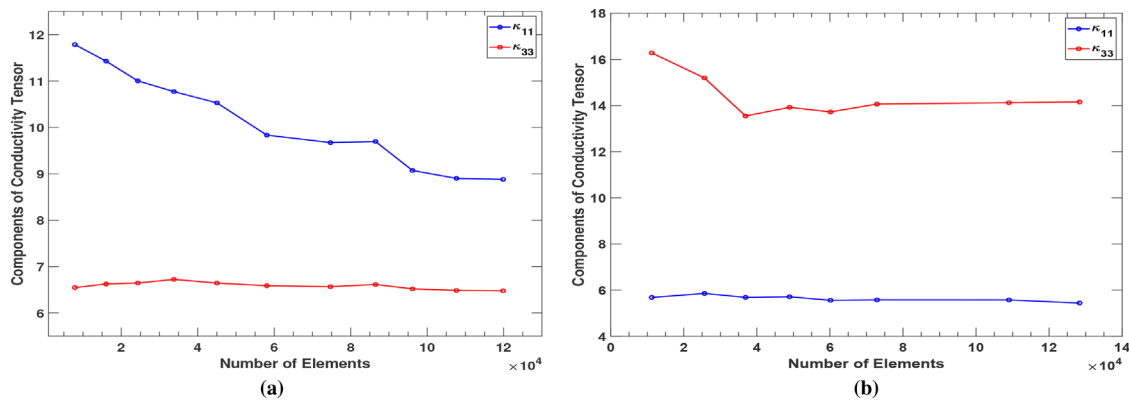


FIG. 9. Mesh convergence study for a unit cell with a spheroidal inclusion with aspect ratios of (a) 0.1 and (b) 10.

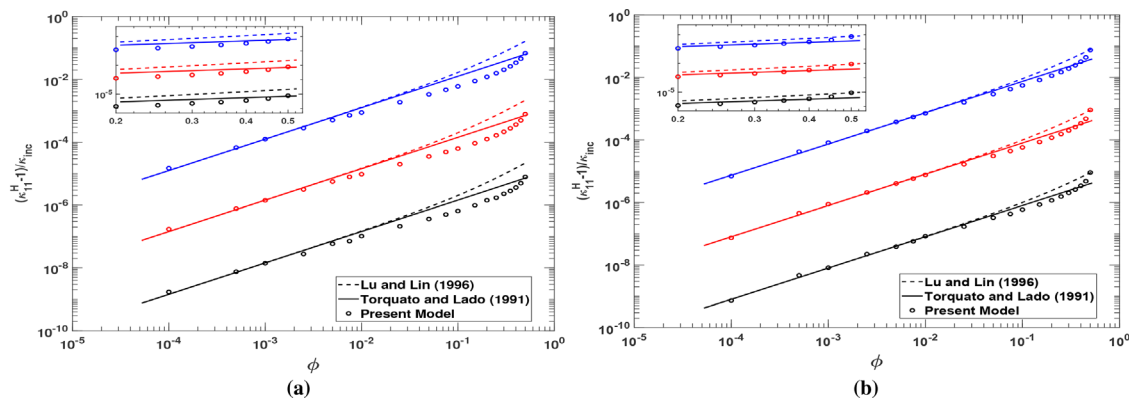
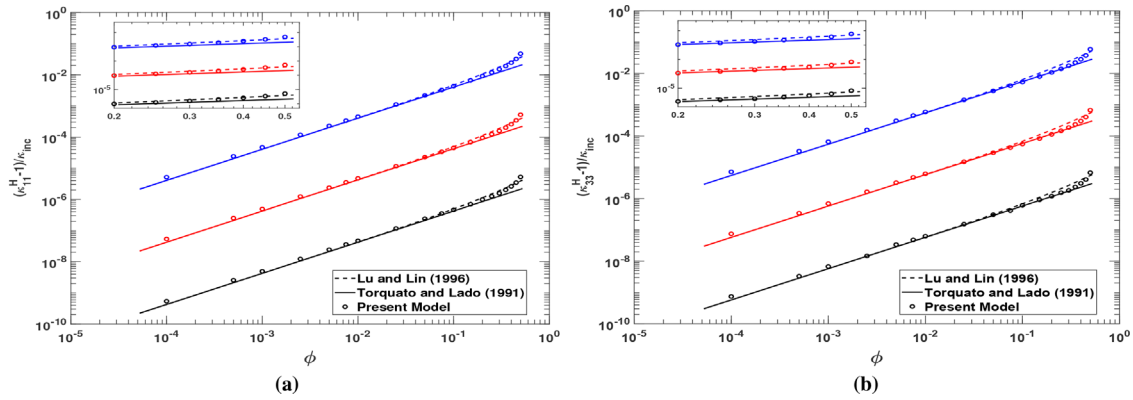
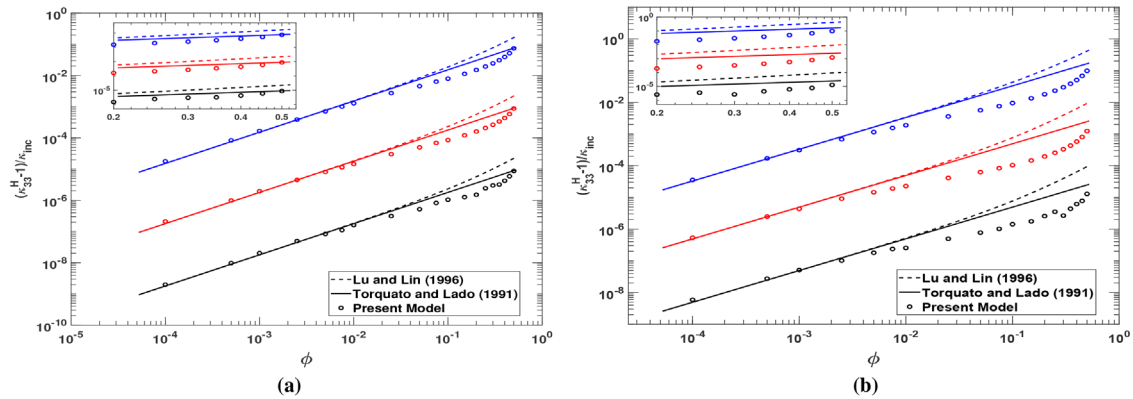


FIG. 10. Plot of  $(\kappa_{11}^H - 1)$  scaled with  $\kappa_{inc}$  as function of volume fraction for spheroidal inclusions having aspect ratios of (a) 0.1 and (b) 0.2 in a simple cubic arrangement. The solid line represents the Torquato and Lado (1991)<sup>25</sup> predictions, and dashed lines represent Lu and Lin's (1996)<sup>26</sup> expression, while the results from present model are plotted using the circle symbol for the different conductivity ratios. The color scheme is same as mentioned in Fig. 3. The inset shows the plot of  $(\kappa_{11}^H - 1)$  scaled with  $\kappa_{inc}$  for  $\phi > 0.2$ .



**FIG. 11.** (a) Plot of  $(\kappa_{11}^H - 1)$  scaled with  $\kappa_{inc}$  as function of volume fraction for spheroidal inclusions of aspect ratio of 0.5 and (b) plot of  $(\kappa_{33}^H - 1)$  scaled with  $\kappa_{inc}$  as function of volume fraction for spheroidal inclusions of aspect ratio of 2 in a simple cubic arrangement. The solid line represents the Torquato and Lado (1991)<sup>25</sup> predictions, and dashed lines represent the Lu and Lin's (1996)<sup>26</sup> expression, while the results from present model are plotted using the circle symbol for the different conductivity ratios. The color scheme is same as mentioned in Fig. 3. The inset in (a) shows the plot of  $(\kappa_{11}^H - 1)$  scaled with  $\kappa_{inc}$  and in (b) the plot of  $(\kappa_{33}^H - 1)$  scaled with  $\kappa_{inc}$  for  $\phi > 0.2$ .



**FIG. 12.** Plot of  $(\kappa_{33}^H - 1)$  scaled with  $\kappa_{inc}$  as function of volume fraction for spheroidal inclusions having aspect ratios of (a) 5 and (b) 10 in a simple cubic arrangement. The solid line represents the Torquato and Lado (1991) predictions, and dashed lines represent Lu and Lin's (1996)<sup>25</sup> expression, while the results from present model are plotted using the circle symbol for the different conductivity ratios. The color scheme is same as mentioned in Fig. 3. The inset shows the plot of  $(\kappa_{33}^H - 1)$  scaled with  $\kappa_{inc}$  for  $\phi > 0.2$ .

oblate and the  $y_3$  axis for prolate). The results obtained from the present model for spheroidal inclusions are compared with the estimates provided by Lu and Lin<sup>26</sup> for the well-stirred models, in which the particles are assumed to take nonoverlapping positions with equal probability, and the interactions between only two inclusions are considered. From the Figs. 10–12, it is clearly seen that the results predicted by the present model agree very well with analytical results for dilute volume fractions. As expected, at higher packing fractions, the effective conductivity is not a linear function of the volume fraction of inclusion but a quadratic one. This trend is again captured very well by the present model.

As seen from Figs. 10(a), 12(a), and 12(b), the deviation seen in the predicted results can be due to the fact that only the first correction term to the scalar potential field is considered. For a prolate or an oblate spheroid, the interparticle interactions are now a function of the aspect ratio and the characteristic length of the inclusion.<sup>7</sup> Though the perturbation of the potential field produced by the close proximity of the inclusions is captured by the first corrections, finer perturbations

to the field, which occur at a length scale much smaller than the length scale of the microstructure, are neglected. Considering these finer perturbations could improve the predicted effective property. The addition of the higher-order term to predict the effective property is proposed to be carried out as future research work.

It is to be noted that the estimates provided by Lu and Lin, which considered only the interactions between a pair of inclusions, were only up to  $\mathcal{O}(\phi^2)$  term. Deviations from the results predicted near the maximum packing fraction could be due to the limitation of Lu and Lin's formulation, which does not consider the contribution of multibody interactions. From the data obtained from the simulations, a correlation function in volume fraction  $\phi$  and conductivity ratio  $\kappa_r$  is given in Tables IV and V. The obtained function provides a  $\mathcal{O}(\phi^4)$  correction to the effective conductivity for any arbitrary conductivity ratio  $\kappa_r$ . Interested readers are requested to use Torquato and Lado's<sup>25</sup> or Lu and Lin's<sup>26</sup> formulations for up to a  $\phi$  of 0.05, and for  $\phi > 0.05$ , readers can use the provided correlation functions.

TABLE IV. Correlation function for prolate spheroids.

Aspect ratio	Correlation function
1.25	$1 + 0.707 \log \kappa_r (\phi + 7.863\phi^2 - 38.09\phi^3 + 63.4\phi^4) \times (1 + 0.21 \log \kappa_r) / (1 + 0.062 \log \kappa_r^2)$
2	$1 + 0.868 \log \kappa_r (\phi + 7.112\phi^2 - 39.31\phi^3 + 66.69\phi^4) \times (1 + 0.308 \log \kappa_r) / (1 + 0.071 \log \kappa_r^2)$
5	$1 + 1.977 \log \kappa_r (\phi + 1.067\phi^2 - 13.01\phi^3 + 28.7\phi^4) \times (1 + 0.103 \log \kappa_r) / (1 + 0.033 \log \kappa_r^2)$
10	$1 + 1.977 \log \kappa_r (\phi + 1.067\phi^2 - 13.01\phi^3 + 28.7\phi^4) \times (1 + 0.103 \log \kappa_r) / (1 + 0.033 \log \kappa_r^2)$

TABLE V. Correlation function for oblate spheroids.

Aspect ratio	Correlation function
0.8	$1 + 0.344 \log \kappa_r (\phi + 26.51\phi^2 - 126.7\phi^3 + 198.1\phi^4) \times (1 + 0.258 \log \kappa_r) / (1 + 0.064 \log \kappa_r^2)$
0.5	$1 + 0.797 \log \kappa_r (\phi + 5.737\phi^2 - 29.84\phi^3 + 51.55\phi^4) \times (1 + 0.335 \log \kappa_r) / (1 + 0.085 \log \kappa_r^2)$
0.2	$1 + 0.429 \log \kappa_r (\phi + 33.7\phi^2 - 170.2\phi^3 + 262.3\phi^4) \times (1 + 0.175 \log \kappa_r) / (1 + 0.043 \log \kappa_r^2)$
0.1	$1 + 1.065 \log \kappa_r (\phi + 4.759\phi^2 - 28.49\phi^3 + 52.49\phi^4) \times (1 + 0.273 \log \kappa_r) / (1 + 0.061 \log \kappa_r^2)$

#### IV. CONCLUSIONS

In this work, for composites having a periodic structure or suspensions with periodically aligned inclusions, the AHM was used to predict the effective conductivity of a heterogeneous media. For the validation of the proposed model, the results of a cylindrical inclusion are compared with Mori-Tanaka and Keller's expressions for close-packed cylinders and were found to agree well with the expressions at the respective packing limits. This study was further extended to include more general shapes and was compared with the existing expressions for various conductivity ratios given in the literature.<sup>26</sup> As observed earlier, the deviations of the predicted result from the existing analytical expressions could be addressed by taking into account the higher-order terms for defining the scalar potential field, which is seen as a scope of future work.

As mentioned earlier, simulations were performed for spheroidal inclusions with moderate aspect ratios and, as an immediate extension of the current work, to implement the AHM to predict the effective conductivity of inclusions that have very high aspect ratios and to systematically compare them with the analytical and experimental results.<sup>4,7,46–48</sup> As noted by Mackaplow *et al.*<sup>47</sup> for highly conducting inclusions near the semidilute regimes, the screening length as described by the author is independent of the orientation and distribution at these concentration limits. Thus, comparing the results obtained by the proposed model would further demonstrate the ability of the same to predict the effective property for very thin fibers as well, which are predominantly present in many metal-filled composites.

These validations and comparisons of the obtained results using the AHM confirm that this multiscale analysis can be systematically used to predict other conductivity-like transport coefficients, such as dielectric constant and magnetic permeability, to name a few. Thus, the AHM coupled with FE is a potential candidate to predict the effective properties of multiphysics problems, such as predicting the effective magnetoelastic properties for a magnetostrictive inclusion in a soft elastic matrix, viscoelastic properties of hydrogels, and rheological properties of complex fluids.

#### ACKNOWLEDGMENTS

The funding received from the Institute of Eminence Research Initiative Projects on Materials and Manufacturing for Futuristic Mobility (project no. SB20210850MMMHRD008275) and the Complex Systems and Dynamics Group (project no. SB20210838AMMHRD008291) is gratefully acknowledged. The authors also extend their gratitude to Professor M. S. Sivakumar, Department of Applied Mechanics, Indian Institute of Technology Madras, for fruitful technical discussions.

E.M.K. thanks Dr. S. Sudersan, Smart Material Characterization Lab, Department of Applied Mechanics, Indian Institute of Technology Madras, for his input and technical discussions. The authors acknowledge using the computing resources at HPCE, IIT Madras.

#### AUTHORS' DECLARATIONS

##### Conflicts of Interest

The authors have no conflicts of interest to disclose.

#### DATA AVAILABILITY

The data that support the findings of this study are available from the corresponding author upon reasonable request.

#### REFERENCES

- <sup>1</sup>A. Einstein, "Berichtigung zu meiner arbeit: Eine neue bestimmung der moleküldimensionen," *Ann. Phys.* **339**, 591 (1911).
- <sup>2</sup>G. Batchelor, "The stress generated in a non-dilute suspension of elongated particles by pure straining motion," *J. Fluid Mech.* **46**, 813–829 (1971).
- <sup>3</sup>A. Acrivos and E. S. G. Shaqfeh, "The effective thermal conductivity and elongational viscosity of a nondilute suspension of aligned slender rods," *Phys. Fluids* **31**, 1841–1844 (1988).
- <sup>4</sup>R. R. Sundararajakumar, D. L. Koch, and E. S. G. Shaqfeh, "The extensional viscosity and effective thermal conductivity of a dispersion of aligned disks," *Phys. Fluids* **6**, 1955–1962 (1994).
- <sup>5</sup>D. L. Koch and J. F. Brady, "The effective diffusivity of fibrous media," *AIChE J.* **32**, 575–591 (1986).

- <sup>6</sup>D. L. Koch and J. F. Brady, "The symmetry properties of the effective diffusivity tensor in anisotropic porous media," *Phys. Fluids* **30**, 642–650 (1987).
- <sup>7</sup>E. S. G. Shaqfeh, "A nonlocal theory for the heat transport in composites containing highly conducting fibrous inclusions," *Phys. Fluids* **31**, 2405–2425 (1988).
- <sup>8</sup>R. T. Bonnecaze and J. F. Brady, "A method for determining the effective conductivity of dispersions of particles," *Proc. R. Soc. London, Ser. A* **430**, 285–313 (1990).
- <sup>9</sup>L. Spielman and S. L. Goren, "Model for predicting pressure drop and filtration efficiency in fibrous media," *Environ. Sci. Technol.* **2**, 279–287 (1968).
- <sup>10</sup>T. Mori and K. Tanaka, "Average stress in matrix and average elastic energy of materials with misfitting inclusions," *Acta Metall.* **21**, 571 (1973).
- <sup>11</sup>R. Hill, "A self-consistent mechanics of composite materials," *J. Mech. Phys. Solids* **13**, 213 (1965).
- <sup>12</sup>G. Papanicolaou, A. Bensoussan, and J.-L. Lions, *Asymptotic Analysis for Periodic Structures* (Elsevier, 1978).
- <sup>13</sup>N. Charalambakis, "Homogenization techniques and micromechanics. A survey and perspectives," *Appl. Mech. Rev.* **63**, 030803 (2010).
- <sup>14</sup>J. Maxwell, *A Treatise on Electricity and Magnetism* (Clarendon Press, 1873), Vol. 1.
- <sup>15</sup>A. Rocha and A. Acrivos, "On the effective thermal conductivity of dilute dispersions, general theory for inclusions of arbitrary shape," *Q. J. Mech. Appl. Math.* **26**, 217 (1973).
- <sup>16</sup>D. J. Jeffrey, "Conduction through a random suspension of spheres," *Proc. R. Soc. London, Ser. A* **335**, 355 (1973).
- <sup>17</sup>J. Keller, "Conductivity of a medium containing a dense array of perfectly conducting spheres or cylinders or nonconducting cylinders," *J. Appl. Phys.* **34**, 991 (1963).
- <sup>18</sup>G. K. Batchelor and R. W. O'Brien, "Thermal or electrical conduction through a granular material," *Proc. R. Soc. London, Ser. A* **355**, 313 (1977).
- <sup>19</sup>L. Rayleigh, "LVI. On the influence of obstacles arranged in rectangular order upon the properties of a medium," *London, Edinburgh, Dublin Philos. Mag. J. Sci.* **34**, 481–502 (1892).
- <sup>20</sup>R. C. McPhedran and D. R. McKenzie, "The conductivity of lattices of spheres. I. The simple cubic lattice," *Proc. R. Soc. London, Ser. A* **359**, 45–63 (1978).
- <sup>21</sup>A. S. Sangani, A. Acrivos, and G. K. Batchelor, "The effective conductivity of a periodic array of spheres," *Proc. R. Soc. London, Ser. A* **386**, 263–275 (1983).
- <sup>22</sup>M. Zuzovsky and H. Brenner, "Effective conductivities of composite materials composed of cubic arrangements of spherical particles embedded in an isotropic matrix," *Z. Angew. Math. Phys.* **28**, 979–992 (1977).
- <sup>23</sup>H.-S. Chen and A. Acrivos, "On the effective thermal conductivity of dilute suspensions containing highly conducting slender inclusions," *Proc. R. Soc. London, Ser. A* **349**, 261 (1976).
- <sup>24</sup>S.-Y. Lu and S. Kim, "Effective thermal conductivity of composites containing spheroidal inclusions," *AIChE J.* **36**, 927 (1990).
- <sup>25</sup>S. Torquato and F. Lado, "Trapping constant, thermal conductivity, and the microstructure of suspensions of oriented spheroids," *J. Chem. Phys.* **94**, 4453 (1991).
- <sup>26</sup>S. Lu and H. Lin, "Effective conductivity of composites containing aligned spheroidal inclusions of finite conductivity," *J. Appl. Phys.* **79**, 6761 (1996).
- <sup>27</sup>P. Suquet, "Elements of homogenization for inelastic solid mechanics, homogenization techniques for composite media," *Lect. Notes Phys.* **272**, 193 (1987).
- <sup>28</sup>S. Torquato, *Random Heterogeneous Materials: Microstructure and Macroscopic Properties* (Springer, 2002), Vol. 55, pp. B62–B63.
- <sup>29</sup>P. Kanoute, D. Boso, J. Chaboche, and B. Schrefler, "Multiscale methods for composites: A review," *Arch. Comput. Methods Eng.* **16**, 31 (2009).
- <sup>30</sup>A. L. Kalamkarov, I. V. Andrianov, and V. V. Danishevskyy, "Asymptotic homogenization of composite materials and structures," *Appl. Mech. Rev.* **62**, 030802 (2009).
- <sup>31</sup>J. Castellero, J. Otero, R. Ramos, and A. Bourgeat, "Asymptotic homogenization of laminated piezocomposite materials," *Int. J. Solids Struct.* **35**, 527 (1998).
- <sup>32</sup>J. Bravo-Castillero, R. Rodríguez-Ramos, H. Mechkour, J. A. Otero, and F. J. Sabina, "Homogenization of magneto-electro-elastic multilaminated materials," *Q. J. Mech. Appl. Math.* **61**, 311 (2008).
- <sup>33</sup>J. Bravo-Castillero, H. Mechkour, J. Otero, J. Cabanas, L. Sixto, R. Guinovart Díaz, and F. Sabina, "Homogenization and effective properties of periodic thermomagnetoelastic composites," *J. Mech. Mater. Struct.* **4**, 819 (2009).
- <sup>34</sup>J. Rubinstein and S. Torquato, "Flow in random porous media: Mathematical formulation, variational principles, and rigorous bounds," *J. Fluid Mech.* **206**, 25–46 (1989).
- <sup>35</sup>N. Takano, M. Zako, T. Okazaki, and K. Terada, "Microstructure-based evaluation of the influence of woven architecture on permeability by asymptotic homogenization theory," *Compos. Sci. Technol.* **62**, 1347–1356 (2002).
- <sup>36</sup>Y. Song and J. Youn, "Asymptotic expansion homogenization of permeability tensor for plain woven fabrics," *Composites, Part A* **37**, 2080–2087 (2006).
- <sup>37</sup>J. Rubinstein and S. Torquato, "Diffusion-controlled reactions: Mathematical formulation, variational principles, and rigorous bounds," *J. Chem. Phys.* **88**, 6372–6380 (1988).
- <sup>38</sup>J.-L. Auriault and J. Lewandowska, "Effective diffusion coefficient: From homogenization to experiment," *Transp. Porous Media* **27**, 205–223 (1997).
- <sup>39</sup>D. Lee and J. Lee, "Comparison and validation of numerical homogenization based on asymptotic method and representative volume element method in thermal composites," *Multiscale Sci. Eng.* **3**, 165 (2021).
- <sup>40</sup>E. Andreassen and C. S. Andreassen, "How to determine composite material properties using numerical homogenization," *Comput. Mater. Sci.* **83**, 488 (2014).
- <sup>41</sup>F. Fantoni, A. Bacigalupo, and M. Paggi, "Multi-field asymptotic homogenization of thermo-piezoelectric materials with periodic microstructure," *Int. J. Solids Struct.* **120**, 31 (2017).
- <sup>42</sup>T. A. Dutra, R. T. L. Ferreira, H. B. Resende, A. Guimarães, and J. M. Guedes, "A complete implementation methodology for asymptotic homogenization using a finite element commercial software: Preprocessing and postprocessing," *Compos. Struct.* **245**, 112305 (2020).
- <sup>43</sup>R. Penta and A. Gerisch, "Investigation of the potential of asymptotic homogenization for elastic composites via a three-dimensional computational study," *Comput. Visualization Sci.* **17**, 185 (2015).
- <sup>44</sup>P. Sonneveld, W. Visscher, F. Panneflek, E. Barendrecht, and M. Michels, "The conductance of suspensions with conducting particles," *J. Appl. Electrochem.* **22**, 935–949 (1992).
- <sup>45</sup>A. Caradonna, C. Badini, E. Padovano, and M. Pietroluongo, "Electrical and thermal conductivity of epoxy-carbon filler composites processed by calendaring," *Materials* **12**, 1522 (2019).
- <sup>46</sup>G. H. Fredrickson and E. S. G. Shaqfeh, "Heat and mass transport in composites of aligned slender fibers," *Phys. Fluids* **1**, 3–20 (1989).
- <sup>47</sup>M. B. Mackaplow, E. S. G. Shaqfeh, and R. L. Schiek, "A numerical study of heat and mass transport in fibre suspensions," *Proc. Roy. Soc. London, Ser. A* **447**, 77–110 (1994).
- <sup>48</sup>R. R. Sundararajakumar and D. L. Koch, "Electrical conductivity of isotropic fibre suspensions," *Proc. Roy. Soc. London, Ser. A* **455**, 1923–1930 (1999).